

# Raman scattering study of anomalous spin-, charge-, and lattice-dynamics in the charge-ordered phase of $\text{Bi}_{1-x}\text{Ca}_x\text{MnO}_3$ ( $x > 0.5$ )

S. Yoon<sup>1</sup>, M. Rübhausen<sup>1</sup>, S. L. Cooper<sup>1</sup>, K. H. Kim<sup>2,3</sup>, and S-W. Cheong<sup>2,4</sup>

<sup>1</sup>*Department of Physics and Frederick Seitz Materials Research Laboratory,  
University of Illinois at Urbana-Champaign, Urbana, IL 61801*

<sup>2</sup>*Department of Physics and Astronomy, Rutgers University, Piscataway, NJ 08854*

<sup>3</sup>*Department of Physics, Seoul National University, Seoul 151-742, Korea*

<sup>4</sup>*Bell Laboratories, Lucent Technologies, Murray Hill, NJ 07974*

(February 1, 2008)

We report an inelastic light scattering study of the effects of charge-ordering on the spin-, charge-, and lattice-dynamics in  $\text{Bi}_{1-x}\text{Ca}_x\text{MnO}_3$  ( $x > 0.5$ ). We find that charge-ordering results in anomalous phonon behavior, such as the appearance of ‘activated’ modes. More significantly, however, the transition to the CO phase results in the appearance of a quasielastic scattering response with the symmetry of the spin chirality operator ( $T_{1g}$ ); this scattering response is thus indicative of magnetic or chiral spin fluctuations in the AFM charge-ordered phase.

PACS numbers: 78.30.-j, 75.30.-m

Among the most interesting and rich phenomena exhibited by complex transition metal oxides such as the nickelates [1], cuprates [2], and manganites [3] is charge- and orbital-ordering, i.e., the organization of charges and orbital configurations in periodic arrays on the lattice. The considerable recent effort devoted to understanding this behavior has revealed a variety of interesting properties, including novel states of matter such as coexisting magnetic phases [4,5] and possible ‘quantum liquid crystal’ states [6]. Yet, a number of important issues remain unsolved, including the effects of orbital and charge ordering (CO) on the lattice and charge dynamics, and the nature of carrier motion in the complex spin background of the Néel state. A clarification of these issues demands experimental methods capable of probing the strong interplay among the spin-, charge-, lattice-, and orbital-degrees-of-freedom in strongly-correlated systems.

In this Letter, we discuss an inelastic light (Raman) scattering study of the unconventional lattice-, spin-, and charge-dynamics in the CO phase of the  $\text{Bi}_{1-x}\text{Ca}_x\text{MnO}_3$  ( $x > 0.5$ ) system. Raman scattering offers several unique features in the investigation of charge-ordered systems. For example, by providing energy, symmetry, and lifetime information concerning lattice-, spin-, as well as charge-excitations, Raman scattering affords unique insight into the interplay among these coupled excitations in various phases. Also, as a technique that can sensitively probe unconventional charge- and spin-dynamics, such as exotic “chiral” spin and charge currents [7–9], Raman scattering offers a unique means of probing the unconventional spin- and charge-dynamics that arise when charge-carriers are placed in the complex spin environment of CO systems.

These benefits are clearly evident in the present study, which uncovers several interesting features of CO behavior in  $\text{Bi}_{1-x}\text{Ca}_x\text{MnO}_3$  ( $x > 0.5$ ). First, polarized Raman measurements show that charge-ordering results in

the appearance of activated phonon modes, due to the lowering of symmetry by charge-stripe formation. Most interesting, however, is the observation that a quasielastic Raman scattering response, with the symmetry of the spin chirality operator ( $T_{1g}$ ), develops in the CO phase. This distinctive scattering response indicates the presence of chiral fluctuations at finite temperatures in the CO/AFM phase, possibly arising from a chiral spin-liquid state associated with the Mn core spins, or from closed-loop charge motion caused by the constraining environment of the complex orbital and Néel spin textures.

The samples used in our study were flux-grown single crystalline  $\text{Bi}_{0.19}\text{Ca}_{0.81}\text{MnO}_3$  ( $T_{\text{co}} = 165$  K,  $T_{\text{N}} = 120$  K) and  $\text{Bi}_{0.18}\text{Ca}_{0.82}\text{MnO}_3$  ( $T_{\text{co}} = 210$  K,  $T_{\text{N}} = 160$  K). The typical dimensions of these samples are  $2 \times 2 \times 1$  mm<sup>3</sup>. Raman spectra were measured in a backscattering geometry using continuous helium flow and cold-finger optical cryostats, and a modified subtractive-triple-grating spectrometer equipped with a nitrogen-cooled CCD array detector. The spectra were corrected for the spectral response of the spectrometer and the detector. The samples were excited with 4 mW of the 4762-Å line of the  $\text{Kr}^+$  laser, focused to a 50  $\mu\text{m}$  diameter spot within a single CO domain of the crystals. Temperatures listed for the Raman spectra include estimates of laser heating effects. To identify excitation symmetries, the spectra were obtained with the incident ( $\mathbf{E}_i$ ) and scattered ( $\mathbf{E}_s$ ) light polarized in various configurations, including ( $\mathbf{E}_i, \mathbf{E}_s$ ) = ( $\mathbf{x}, \mathbf{x}$ ) and ( $\mathbf{y}, \mathbf{y}$ ):  $A_{1g} + E_g$ , and ( $\mathbf{E}_i, \mathbf{E}_s$ ) = ( $\mathbf{L}, \mathbf{L}$ ):  $A_{1g} + \frac{1}{4}E_g + T_{1g}$ , where  $\mathbf{x}$  and  $\mathbf{y}$  are the [100] and [010] crystal directions, respectively,  $\mathbf{L}$  is left circular polarization, and where  $A_{1g}$ ,  $E_g$  and  $T_{1g}$  are respectively the singly-, doubly-, and triply-degenerate irreducible representations of the  $O_h$  space group of the crystals, which have a pseudocubic structure [10–13].

Figure 1 (a) shows polarized microscope images of the

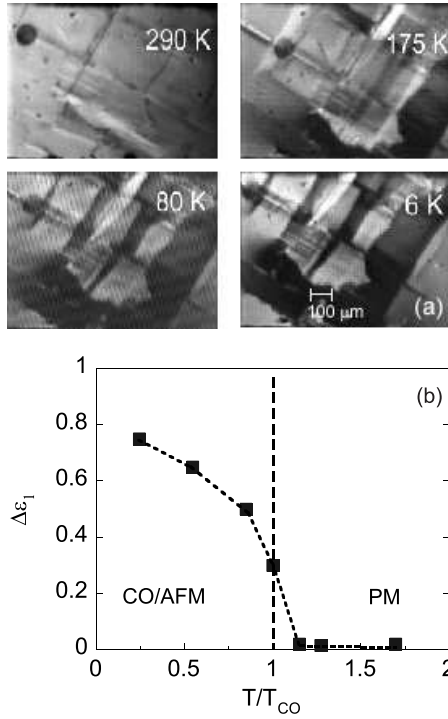


FIG. 1. (a) Polarized microscope images of developing CO domains at various temperatures. (b) Dielectric anisotropy parameter  $\Delta\epsilon_1$  (see text) at  $\omega = 1$  eV. The dotted line is a guide to the eye.

(100)  $\text{Bi}_{0.19}\text{Ca}_{0.81}\text{MnO}_3$  sample surface taken at 290 K, 175 K, 80 K, and 6 K, respectively. One can clearly see the growth of “light” and “dark” regions below the charge-ordering temperature,  $T_{\text{co}} = 165$  K, corresponding to the development of domains having perpendicular orientations of the charge-strips. The evolution of CO behavior and domain formation below  $T_{\text{co}}$  is more quantitatively illustrated in Fig. 1 (b), which presents the temperature dependence of the dielectric anisotropy,  $\Delta\epsilon_1(\omega) = \frac{|\epsilon_1^{ac} - \epsilon_1^{bc}|}{\sqrt{(\epsilon_1^{ac})^2 + (\epsilon_1^{bc})^2}}$ , where  $\epsilon_1^{ac}$  and  $\epsilon_1^{bc}$  are the dielectric responses for  $\omega = 1$  eV light polarized in the ac and bc planes respectively [14]. Notably, the temperature-dependence of  $\Delta\epsilon_1$  is similar to that of the order-parameter in a second-order phase transition, consistent with our expectation that the increasing size of this quantity below  $T_{\text{co}}$  reflects the increasing organization of charges below  $T_{\text{co}}$ . However, at low temperatures,  $\Delta\epsilon_1$  saturates below the maximum value of 1 due to the fact that the optical spot in the ellipsometry measurements is not isolated to a single domain.

One of the distinct advantages of polarized Raman scattering techniques for measuring optical anisotropy in the CO phase is that this technique allows the study of single ( $\lesssim 100 \mu\text{m}$ ) domains with uniformly aligned charge stripes. Raman spectra of single domain regions in  $\text{Bi}_{0.19}\text{Ca}_{0.81}\text{MnO}_3$  are illustrated, for various temperatures and scattering geometries, in Fig. 2. Note first that in the high temperature “isotropic” phase ( $T = 305$  K),

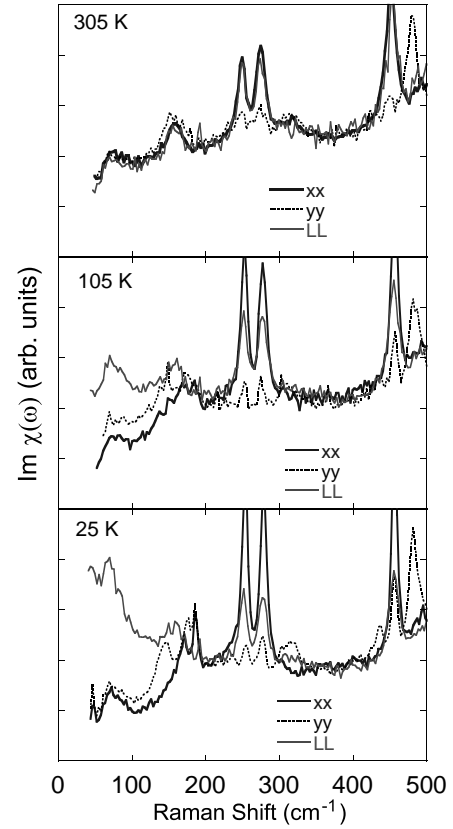


FIG. 2. Raman spectra of  $\text{Bi}_{0.19}\text{Ca}_{0.81}\text{MnO}_3$  in xx, yy and LL polarization configurations at 305 K, 105 K, and 25 K.

all three scattering geometries (xx, yy, and LL) overlap, with the exception of some intensity differences associated with the phonons. However, with decreasing temperature into the CO phase, two significant features are evident: First, several changes in the phonon spectra evolve with decreasing temperature, including the appearance of new modes and the evolution of differences in the phonon spectra associated with the xx and yy scattering geometries. Second, while the low frequency backgrounds associated with the xx and yy scattering geometries decrease with decreasing temperature into the CO phase, there is a dramatic growth of the low frequency scattering background in the LL geometry, betraying the development of a distinctive  $T_{1g}$ -symmetry quasielastic scattering response in the CO/AFM phase.

We focus first on the effects of charge-ordering on the phonons in  $\text{Bi}_{0.19}\text{Ca}_{0.81}\text{MnO}_3$  - such information is important, as the optical phonons function as ‘local probes’ of changes in the local symmetry and bond-strengths caused by charge-ordering [15]. Consider first the  $\sim 160 \text{ cm}^{-1}$   $A_{1g}$  phonon mode in Fig. 3 (circles and triangles), which is associated with in-phase Mn vibrations. This mode exhibits an abrupt hardening across the charge-ordering transition, indicative of the effects of charge-ordering on the lattice force constants via changes in the Coulomb energies. Also, Figs. 2 and 3 illustrate the ap-

pearance of a second mode at  $\sim 185 \text{ cm}^{-1}$ . In the

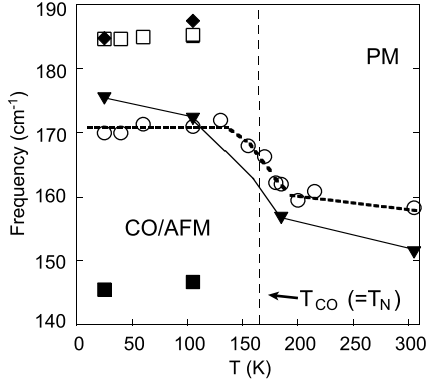


FIG. 3. Hardening of the Mn vibration mode ( $\sim 160 \text{ cm}^{-1}$ ) and the development of additional modes ( $\sim 145 \text{ cm}^{-1}$  and  $\sim 185 \text{ cm}^{-1}$ ) below the CO transition. Open symbols denote data from xx, and filled symbols denote data from yy scattering geometries. The lines are guides to the eye.

isotropic high temperature phase ( $T > T_{\text{co}}$ ), this mode is present in the xy scattering configuration, but develops also in the xx scattering geometry below  $T_{\text{co}}$  due to the breakdown of symmetry selection rules in the CO phase.

The breaking of 4-fold in-plane symmetry due to long-range charge-ordering is also reflected in differences in the phonon spectra observed in the xx and yy scattering geometries. In particular, the yy spectrum at 25 K (Fig. 2) shows the development of ‘new’ phonon modes near  $\sim 145 \text{ cm}^{-1}$  (filled squares in Fig. 3),  $\sim 300 \text{ cm}^{-1}$ , and  $\sim 420 \text{ cm}^{-1}$ . The appearance of new modes can reflect Brillouin-zone-folding of zone boundary modes to the zone center, caused by the additional periodicity associated with charge-stripe formation. It is expected, however, that zone-folded modes should have much weaker intensities than ‘regular’ modes [16,17], which is not the present case. A more plausible interpretation therefore is that the new modes we observe are “activated” modes due to charge-ordering: For example, the out-of-phase Mn vibrational mode is not Raman-active in the PM ‘isotropic’ phase because the net charge fluctuation associated with out-of-phase motion of the ( $\text{Mn}^{3.5+} - \text{O} - \text{Mn}^{3.5+}$ ) complex is zero, and hence this mode cannot modulate the polarizability. However, in the CO phase, the different charges on the  $\text{Mn}^{3+}$  and  $\text{Mn}^{4+}$  sites cause out-of-phase Mn vibrations of the ( $\text{Mn}^{3+} - \text{O} - \text{Mn}^{4+}$ ) complex to have a non-zero net charge fluctuation that couples to the polarizability, resulting in the ‘new’ Raman-active mode at  $145 \text{ cm}^{-1}$ .

An even more interesting feature apparent in Figs. 2 and 4 (a) is the development in the CO state of a quasielastic Raman response in the LL scattering geometry,

$$\text{Im}\chi(\omega) \sim \frac{A\omega\Gamma}{\omega^2 + \Gamma^2} \quad (1)$$

where A is the quasielastic scattering amplitude and  $\Gamma$  is the fluctuation rate. The absence of a similar scattering

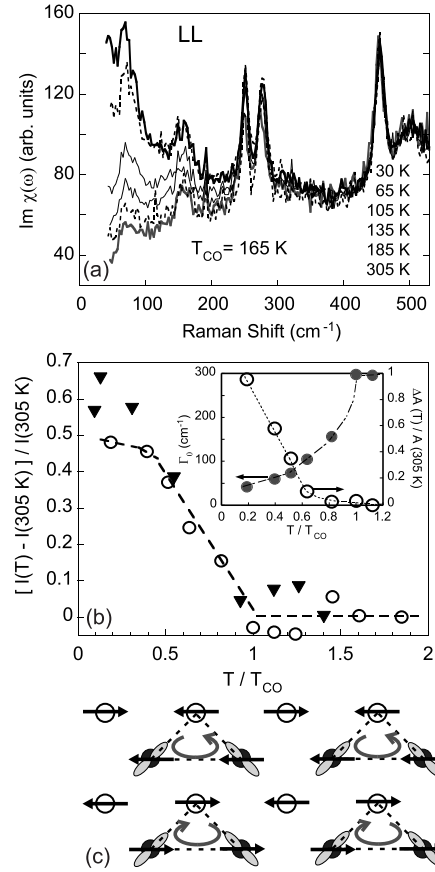


FIG. 4. (a) Temperature dependence of the Raman spectra in the LL scattering geometry. (b) Fractional change in the integrated quasielastic Raman scattering intensity ( $50 - 350 \text{ cm}^{-1}$ ) as a function of temperature for the  $T_{\text{co}} = 165 \text{ K}$  (circles) and  $T_{\text{co}} = 210 \text{ K}$  (triangles) samples. Inset: Fractional change in the quasielastic scattering amplitude A and fluctuation rate  $\Gamma$  as a function of temperature. Lines are guides to the eye. (c) Example of a closed-loop path for charge motion in the CO phase ( $x = 0.5$ ) which is not precluded by either the orbital configuration or by the spin environment. Filled and empty circles represent  $\text{Mn}^{3+}$  and  $\text{Mn}^{4+}$  sites, respectively.

response in either xx or yy scattering geometries definitively identifies this quasielastic response as having  $T_{1g}$  symmetry. This distinctive scattering symmetry transforms like the spin-chirality operator ( $\vec{S}_1 \cdot \vec{S}_2 \times \vec{S}_3$ ) [9], and is typical of scattering from magnetic fluctuations [18] and from chiral spin fluctuations [9]. Thus, while the ground state of the CO/AFM phase is not generally expected to have a net magnetization or spin chirality, the development of this  $T_{1g}$  quasielastic response in Figs. 2 and 4 (a) betrays the presence of strong *fluctuations* associated with such a broken time-reversal symmetry state at finite temperatures in the CO/AFM phase. Interestingly, the fluctuation rate  $\Gamma$  associated with this unusual response (inset Fig. 4 (b)) tends to zero with decreas-

ing temperature, perhaps indicating a tendency toward static long-range order as  $T \rightarrow 0$ .

When considering the origin of this anomalous scattering response, we can first rule out a “precursor” fluctuational response associated with either charge-stripe- or orbital-ordering: while such responses should develop above, become maximum near, and diminish below the ordering transition temperature  $T_{co}$ , Figs. 4 (a) and (b) clearly illustrate that the  $T_{1g}$  quasielastic response we observe evolves at  $T_{co}$ , and grows with decreasing temperature below  $T_{co}$ , coincident with the charge-order-parameter  $\Delta^c$  in Fig. 1 (b).

Several intriguing possibilities are consistent with both the distinctive  $T_{1g}$  symmetry and temperature dependence of the quasielastic light scattering response in Figs. 4 (a) and (b). First, although neutron scattering studies show no evidence for ferromagnetic spin fluctuations below  $T_N$  in this system [13], it is possible that the  $T_{1g}$  scattering we observe reflects spin fluctuations associated with a canted AFM phase. Similarly, the properties of the quasielastic scattering response in Fig. 4 are also consistent with the presence of chiral spin fluctuations associated with the core spins, for example similar to those observed in ferromagnetic pyrochlores such as  $\text{Sm}_2\text{Mo}_2\text{O}_7$  [19]. Such fluctuations of canted AFM or spin chirality could arise in the CO manganites due to geometrical frustration of the Mn core spins, and/or to an appreciable Dzyaloshinskii-Moriya interaction ( $\sim \vec{S}_1 \times \vec{S}_2$ ), in the AFM/CO phase.

Finally, another interesting possibility is that the fluctuational response in Fig. 4 is associated with chiral charge currents, i.e., charges constrained to hop in closed-loop paths. The possibility of such charge motion in the Néel spin environment of the CO/AFM phase is suggested by first noting that long-range translational charge motion is constrained in this phase by the complex orbital and Néel spin structure, by the constraints of the double-exchange hopping mechanism, and by disorder (e.g., by doping away from commensurate fillings), which strongly limits conduction along the 1D  $\text{Mn}^{3+}$  chains [20]. However, Fig. 4 (c) illustrates one possible closed-loop path in which the hopping of holes is not constrained by either the spin or orbital environments in the CO/AFM phase. Interestingly, Nagaosa and Lee predicted that such “closed-loop” charge hopping should be present in doped AFM insulators, and should be manifest in the appearance of a quasielastic Raman response [8] similar to that observed in the CO/AFM phase of  $\text{Bi}_{1-x}\text{Ca}_x\text{MnO}_3$  ( $x > 0.5$ ) (Fig. 4 (a)). Such quasielastic light scattering arises in this case from fluctuations in an induced effective magnetic field generated by the chiral charge currents,  $\langle \chi(m)\chi^\dagger(m) \rangle \sim \langle mm^\dagger \rangle$ , where  $\chi(m)$  is the ‘field’-dependent electric susceptibility.

In conclusion, our Raman scattering studies of  $\text{Bi}_{1-x}\text{Ca}_x\text{MnO}_3$  have allowed us to explore the influence of charge- and orbital-ordering on the lattice-, charge-,

and spin-dynamics. Most significantly, in the CO/AFM phase these studies reveal the development of a fluctuational (quasielastic) response with the distinctive symmetry of the spin-chirality operator – this remarkable response is consistent with the presence of a fluctuating chiral state at finite temperatures in the CO/AFM state. Importantly, these studies also clearly demonstrate that Raman scattering is uniquely suited to probing exotic “chiral” phases in other correlated systems, such as the CMR-phase manganites [21], geometrically-frustrated metallic ferromagnets [19], the high  $T_c$  cuprates [8], and quantum Hall systems.

We thank M. V. Klein, Y. Lyanda-Geller, and P. Goldbart for useful discussions. We acknowledge financial support of the DOE via DEFG02-96ER45439 (S.Y., M.R., S.L.C.), the DFG via Ru 773/1-1, the NSF through the STCS via DMR91-20000 (M.R.), and NSF-DMR-9802513 (K.H.K., S-W.C.).

- 
- [1] C. H. Chen, S-W. Cheong, and A. S. Cooper, *Phys. Rev. Lett.* **71**, 2461 (1993).
  - [2] J. M. Tranquada *et al.*, *Nature (London)* **375**, 561 (1995).
  - [3] C. H. Chen and S-W. Cheong, *Phys. Rev. Lett.* **76**, 4042 (1996).
  - [4] H. L. Liu, S. L. Cooper, and S-W. Cheong, *Phys. Rev. Lett.* **81**, 4684 (1998).
  - [5] A. Moreo, S. Yunoki, and E. Dagotto, *Science* **283**, 2034 (1999).
  - [6] S. A. Kivelson, E. Fradkin, and V. J. Emery, *Nature (London)* **393**, 550 (1998).
  - [7] D. V. Khveshchenko and P. B. Wiegmann, *Phys. Rev. Lett.* **73**, 500 (1994).
  - [8] N. Nagaosa and P. A. Lee, *Phys. Rev. B* **43**, 1233 (1991).
  - [9] B. S. Shastry and B. I. Shraiman, *Phys. Rev. Lett.* **65**, 1068 (1990); P. E. Sulewski *et al.*, *ibid.*, **67**, 3864 (1991).
  - [10] Y. Moritomo *et al.*, *Phys. Rev. B* **55**, 7549 (1997).
  - [11] S. Mori, C. H. Chen, and S-W. Cheong, *Nature (London)* **392**, 473 (1998).
  - [12] P. G. Radaelli *et al.*, *Phys. Rev. B* **55**, 3015 (1997).
  - [13] W. Bao *et al.*, *Phys. Rev. Lett.* **78**, 543 (1997).
  - [14] M. Rübhausen *et al.*, *Phys. Rev. B* **62**, R4782 (2000).
  - [15] K. Yamamoto *et al.*, *J. Phys. Soc. Jpn* **68**, 2538 (1999).
  - [16] E. Ya. Sherman *et al.*, *Europhys. Lett.* **48**, 648 (1999).
  - [17] M. Fischer, *et al.*, *Phys. Rev. B* **60**, 7284 (1999).
  - [18] S. L. Cooper *et al.*, *Phys. Rev. B* **35**, 2615 (1987); S. L. Cooper *et al.*, *ibid.*, **36**, 5743 (1987).
  - [19] Y. Taguchi and Y. Tokura, *Phys. Rev. B* **60**, 10280 (1999); K. Ohgushi *et al.*, *cond-mat/9912206*.
  - [20] R. Maezono, S. Ishihara, and N. Nagaosa, *Phys. Rev. B* **57**, R13993 (1998).
  - [21] S. H. Chun *et al.*, *Phys. Rev. Lett.* **84**, 757 (2000); Y. Lyanda-Geller *et al.*, *cond-mat/9904331*; J. Ye *et al.*, *Phys. Rev. Lett.* **83**, 3737 (1999).